Theoretical Investigation and Reinterpretation of the Decomposition of Lithiated Proline and N-Methyl Proline

A. Mookherjee and P. B. Armentrout*

Department of Chemistry, University of Utah, 315 S.1400 E. Rm 2020, Salt Lake City, UT 84112, United States

ABSTRACT: Lithium cation complexes of proline (Pro) and N-methyl proline (NMP) have been collisionally activated with xenon in a guided ion beam tandem mass spectrometer (GIBMS). In addition to the loss of the intact ligand, Pro and NMP, we observed two prominent fragmentation pathways involving the loss of (CO + LiOH) and (CO + H_2O). Quantum chemical calculations at the B3LYP/6-311+G(d,p) level are used to explore the reaction mechanisms of these Li^+(Pro) and Li^+(NMP) fragmentations. Complete potential energy surfaces including all intermediates and transition states are elucidated for the two fragmentation processes in both systems. Theoretical molecular parameters for the rate-limiting transition states are then used to analyze the experimental data. The experimental threshold energies are compared with single point energies calculated at six different levels of theory. Reasonable agreement between experiment and some levels of theory indicate that loss of the intact amino acid competes with the loss of CO over a tight transition state in both Li^+(Pro) and Li^+(NMP) systems. Once CO is lost, efficient loss of H_2O can occur at lower or comparable energy and is followed at somewhat higher energies by loss of LiOH, both proceeding by loose transition states. Overall, we find that MP2(full)/6-311+G(2d,2p) gives the best agreement with the experimental threshold energies and the qualitative characteristics of the competing reactions. This study refines the bond energy of Li^+ to Pro by considering competition with CO loss and lowers the value previously published by 24 ± 12 kJ/mol, with methylation of proline increasing the bond energy to Li^+ by 9 ± 15 kJ/mol.

Key words: bond dissociation energies, collision-induced dissociation, energy-resolved mass spectrometry, methylation, proline

* Corresponding author. E-mail address: armentrout@chem.utah.edu (P.B.A.).

1. Introduction

More than 30% of the known proteins are metalloproteins [1,2], such that metal cation effects on protein structure are important in many fundamental biological processes. Among the 20 naturally occurring amino acids, proline is unique because its side chain incorporates a pyrrolidine ring, thus yielding a secondary amine. Proline is known to have a significant effect on protein structure and peptide fragmentation in mass spectrometry because of this ring structure [3]. Previously, our laboratory conducted a meticulous examination of alkali cation interactions with proline, allowing a better understanding of the structural characteristics of these five-membered ring complexes [4].

More recently, we have examined the alkali metal cation interactions with N-methyl proline, NMP. Here, we used threshold collision-induced dissociation (TCID) in a guided ion beam tandem mass spectrometer to determine the bond dissociation energies (BDEs) for the gas-phase interactions of four alkali metal cations, Li^+, Na^+, K^+, and Rb^+, with NMP [5]. CID of the M^+(NMP) complexes showed the loss of the intact NMP ligand for $M^+ = Na^+$, K^+, and Rb^+ as the only reaction pathway. For Li^+(NMP), although the loss of the ligand is an entropically favored process observed at high energies, the products are dominated by two other primary reaction pathways occurring at low collision energies: loss of (CO + H_2O) and loss of (CO + LiOH). Analogous reactions were previously observed for Li^+(Pro) by Moision and Armentrout [4]. In order to understand these two fragmentation processes, identify the products, and interpret the threshold energies, the rate-limiting transition states (TS) must be known. The present study identifies these by a rigorous examination of the potential energy surfaces (PESs) to arrive at the reaction mechanism for each fragmentation reaction. These rate-limiting TSs are then used to model the data and extract threshold energies for the reactions. Comparison of these experimental threshold energies with the calculated energies can then be used to confirm the reaction mechanism for each reaction pathway. By comparing the similar decomposition reactions of Li^+(Pro) and Li^+(NMP), we also acquire an understanding of the effect of the additional methyl group in Li^+(NMP).

The importance of elucidating fragmentation processes arises not only from their fundamental interest but also because such understanding provides a more complete and potentially quantitative description of decomposition reactions of relevance in analytical mass spectrometry. Such information can potentially provide useful insight and better models of fragmentation processes, which in turn may allow more accurate and complete identification of the amino acid sequences of peptides and proteins [6-15].

2. Experimental and computational section

2.1. General procedures

The guided ion beam tandem mass spectrometer (GIBMS) used to measure the cross sections for threshold collision-induced dissociation (TCID) of alkali metal cation complexes of Pro and NMP has been described previously in detail [16,17]. Details of the experiment have been discussed elsewhere [4,5]. For both Li^+(Pro) and Li^+(NMP), the data analysis requires consideration of the competition between the different fragmentation channels. Here, cross sections for competing channels j are modeled using a statistical approach [18,19], Eq. (1).

$$\sigma_j(E) = \frac{n\sigma_{0,j}}{E}\sum g_i \int_{E_{0,j}-E_i}^{E} \frac{k_j(E^*)}{k_{tot}(E^*)}\left\{1-e^{-k_{tot}(E^*)\tau}\right\}(E-\varepsilon)^{n-1}\mathrm{d}(\varepsilon) \quad (1)$$

Here $\sigma_{0,j}$ is an adjustable scaling parameter for channel j, n is an adjustable parameter that describes the efficiency of energy deposition during a collision [16], E is the relative kinetic energy of the reactants, $E_{0,j}$ is the threshold for collision-induced dissociation for channel j at 0 K, and ε is the energy transferred from translation to internal energy of the reactant complex during collision. The summation in Eq. (1) is over the rovibrational states of the reactant ions, i, where E_i is the excitation energy of each state and g_i is the fractional population of those states ($\Sigma g_i = 1$). $E^* = \varepsilon + E_i$ is the energy of the energized molecule (EM) after the collision. The term of Eq. (1) in curly brackets is the total probability of dissociation of the EM, P_{D1}, where τ is the experimental time for dissociation, ~ 5×10^{-4} s [16]. Vibrational frequencies and rotational constants of the reactant ions used to calculate E_i and g_i are obtained from quantum-chemical

calculations described in the computational section. The Beyer-Swinehart-Stein-Rabinovitch algorithm [20,21] is used to evaluate the density of the rovibrational states, and the relative populations g_i are calculated for a Maxwell-Boltzmann distribution at 300 K. The terms $k_j(E^*)$ and $k_{tot}(E^*)$ in Eq. (1) are the unimolecular rate constant for dissociation of the EM to channel *j* and the total over all channels. These rate constants are defined by Rice-Ramsperger-Kassel-Marcus (RRKM) theory [22,23], Eq. (2),

$$k_{tot}\ \ E\ \ = \sum k_j(E^*) = \sum \frac{d_j N^{\dagger}_{j,vr}(E^* - E_{0,j})}{h\rho_{vr}(E^*)} \qquad (2)$$

where d_j is the reaction degeneracy for channel *j*, h is Planck's constant, $N^{\dagger}_{j,vr}(E^* - E_{0,j})$ is the sum of the rovibrational states of the transition state (TS) at an energy $E^* - E_{0,j}$ for channel *j*, and $\rho_{vr}(E^*)$ is the density of rovibrational states of the EM at the available energy, E^*. Vibrational frequencies and rotational constants of the EM and TS needed to evaluate Eq. (2) are taken from the quantum chemical calculations below. For reactions limited by loose TSs, most TS frequencies equal those of the dissociated products and the transitional frequencies are treated as rotors in the phase space limit (PSL), as discussed in detail elsewhere [5,18,19]. For reactions limited by tight TSs, molecular parameters are taken from calculations.

The fragmentation of the Li^+(AA) reactant complex to Li^+ + AA (where AA = Pro or NMP) competes with the loss of CO, which proceeds over a tight TS, as found below. Competition between these two channels is included in Eq. (1) by the branching ratio term, $k_j(E^*)/k_{tot}(E^*)$. The loss of CO is followed by the two low-energy fragmentation channels, loss of H_2O and loss of LiOH. These sequential dissociation processes are included in our analysis using a recently developed model [24]. Here the probability for further dissociation is $P_{D2} = 1 - \exp\left[-k_{2tot}(E_2^*)\tau_2\right]$, where k_{2tot} is the total rate coefficient for secondary dissociation, E_2^* is the energy available to the secondary energized molecule EM_2, and τ_2 is the time available for the secondary dissociation. As shown in Eq. (3), the total CID cross section of Eq. (1) is partitioned into a cross section for non-dissociating products in Eq. (3a) and that for the sequential dissociation product ion in Eq. (3b).

UU IR Author Manuscript

$$\sigma_1(E) = \sigma_{CID}(E)\left(1 - P_{D2}\right) \quad (3a)$$

$$\sigma_2(E) = \sigma_{CID}(E)\,P_{D2} \quad (3b)$$

One of the challenges in analyzing the sequential thresholds lies in the fact that the first dissociation process takes away an unknown distribution of energies in the translational modes of the initial products and the internal modes of the neutral product. As a result there is an unknown distribution of internal energies in the ionic product that undergoes further dissociation. The model used here makes a statistical assumption regarding energy deposition in the products of the initial reaction. The internal energy of the primary product ion undergoing sequential dissociation, EM_2, is determined by energy conservation, $E_2^* = E^* - E_0 - T_1 - E_L$, where T_1 is the translational energy of the primary products, and E_L is the internal energy of the neutral product. Rate coefficients for EM_2 are again calculated using RRKM theory, Eq. (2). Importantly, this statistical model for sequential reactions cannot deal appropriately with a primary channel that is limited by a tight transition state because the energy released in going to intermediates beyond may not be distributed statistically. Nevertheless, it is still useful to attempt to analyze such sequential channels using this model, with the proviso that the thresholds may be elevated because more energy is available to the product than the statistical model assumes.

Several effects that obscure our interpretation of data must also be accounted for during the data analysis. Our models represent products formed as a result of a single collision event, which is accounted for by collecting data at three different pressures of Xe and extrapolating to zero pressure of Xe [25]. Before making a comparison with the experimental data, cross sections calculated from Eq. (1) and the sequential model are convoluted over the kinetic energy distributions of the reactant ion and neutral gas, as previously detailed [17,26,27]. A nonlinear least-squares method is used to optimize the values of $\sigma_{0,j}$, n, and $E_{0,j}$. Uncertainties in these parameters are estimated from the range of values that are determined from different data sets and include variations in vibrational frequencies (± 10%), in the parameter n (± 10%), in τ by a factor of 2, in the frequency scaling factor (see results section below), and the uncertainty in the absolute energy scale of 0.05 eV (lab).

UU IR Author Manuscript

2.2. Computational Details

All calculations were performed using the Gaussian 09 suite of programs [28]. Ground structures of the reactants were obtained previously [4,5]. The reaction pathway was determined by calculation of suitable intermediates and connecting transition states. The transition states were determined from relaxed potential energy surface scans performed at the B3LYP/6-31+G(d) level or by the Synchronous Transit-Guided Quasi-Newton (STQN) method [29,30] at the B3LYP/6-311+G(d,p) level of theory. Transition state structures, characterized by an imaginary frequency, were confirmed by locating stable intermediates on either side of the barrier and by performing intrinsic reaction coordinate (IRC) calculations performed at the B3LYP/6-311+G(d,p) level. Final geometry optimization calculations and frequency analysis of all reactants, intermediates, and transition states were done at the B3LYP/6-311+G(d,p) level. The B3LYP/6-311+G(d,p) level has been shown to give accurate descriptions of comparable metal-ligand systems [31-35]. Single point energy calculations for all key structures were carried out at three different levels of theory, B3LYP, B3P86, and MP2(full) using the 6-311+G(2d,2p) basis set. Zero-point vibrational energy (ZPE) corrections were obtained at the B3LYP/6-311+G(d,p) level after scaling by 0.9804 [36]. Basis set superposition errors (BSSE) in Li^+-AA bond energies were estimated using the full counterpoise (cp) method [37].

Because the systems under study include lithium, it is important to consider the effects of correlation of the core electrons on lithium, as has been elucidated elsewhere [38]. Consequently, key intermediates, TSs, and products were also calculated at the MP2(full) level of theory using the cc-pCVDZ basis set for Li^+ that includes core correlation along with cc-pVDZ [39,40] on all other atoms. This is designated as cc-pVDZ(Li─C) below. Single point energies were calculated at B3LYP, B3P86, and MP2(full) levels using the cc-pCVTZ basis set for Li^+ and aug-cc-pVTZ for all other atoms. This is designated as aug-cc-pVTZ (Li─C) below. BSSE corrections were not applied as they are known to reduce the accuracy of the MP2(full) energies [38].

UU IR Author Manuscript

UU IR Author Manuscript

3. Results

3.1. Cross Sections for Collision-Induced Dissociation

Experimental TCID cross sections for the interaction of Xe with Li^+(AA) where AA = Pro and NMP as a function of the collision energy are shown in Figures 1a and 1b [4,5]. Three and five processes are observed in the Li^+(Pro) and Li^+(NMP) systems, respectively. The proposed mechanism for the formation of each product from Li^+(Pro) (X = H) and Li^+(NMP) (X = CH_3) is shown in Scheme 1. For both systems, there are two low-energy pathways corresponding to loss of CO and either H_2O or LiOH. (Exact mass measurements utilizing a Fourier transform ion cyclotron resonance, FTICR, mass spectrometer also observe these two products as the major decomposition channels and verify their identity in the Li^+(Pro) system as shown in the Supplementary Data.) In the case of Li^+(NMP), the primary ion formed by CO loss was explicitly looked for and could not be located. A similar result seems likely for the previously published Li^+(Pro) system [4], but confirmation comes from the FTICR results, which also do not observe loss of only CO. It is possible that the loss of CO is followed very closely by the loss of H_2O or LiOH such that the magnitude of this primary product is too small to be observed. The losses of (CO + H_2O) and (CO + LiOH) are also observed in other lithiated biomolecules [41]. At higher energies, the Li^+(Pro) products are dominated by loss of the intact amino acid to form Li^+, whereas this is a much smaller product in the Li^+(NMP) system, consistent with the lower apparent thresholds for the two low-energy decomposition channels.

In the Li^+(NMP) system, two minor products were also observed, Figure 1b. A product rising at a similar energy to Li^+ is $Li^+(H_2O)$, which is formed by loss of CO and C_5H_9N from Li^+(NMP). The formation of $Li^+(H_2O)$ is a commonly observed reaction in the fragmentation of certain lithium ion complexes [42,43]. At higher energies, the product $C_2H_6N^+$ is formed, Figure 1b, and is likely to be the result of a sequential loss of propyne (possibly allene) from the $C_5H_{10}N^+$ product ion formed by (CO + LiOH) loss. The analogous product ions, $Li^+(H_2O)$ and CH_4N^+, were not observed in the Li^+(Pro) system. This is consistent with the smaller magnitudes of the cross sections for loss of (CO + H_2O), the channel that competes directly with $Li^+(H_2O)$

formation, and for loss of (CO + LiOH), which gives the primary product that then would dissociate to give CH_4N^+. Thus, both of these minor products in the Li^+(Pro) system would have maximum cross sections near the noise level. In the Li^+(Pro) system, the FTICR experiment also observed a very small amount of CO_2 loss, Figure S2 of the Supplementary Data, consistent with the zwitterionic structure identified previously for this species [4]. The small magnitude of this product ion suggests that this product should have been below our detection limit in both the Li^+(Pro) and Li^+(NMP) systems.

Finally, we also observed a small product corresponding to the loss of H_2O in the NMP system (as shown in Figure S1) and such a product was also observed for the Pro system using FTICR, Figure S2. As discussed in the Supplementary Data, these processes appear to result from a water adduct of a contaminant or rearranged Li^+(AA) formed in the source, which has been observed for other lithiated amino acids [44,45]. Because these products do not result from decomposition of the intact Li^+(AA) complexes, they should not be included in the following analysis.

Overall, there are two primary decomposition pathways for Li^+(AA) observed for both Pro and NMP: the loss of CO and the loss of AA. The CO loss product then decomposes rapidly by subsequent loss of H_2O or LiOH. These latter channels involve backbone cleavage of the amino acids, which potentially has implications for the use of metallation in sequencing peptides by mass spectrometric methods. It is interesting to note that, in both systems, the cross section corresponding to the loss of (CO + H_2O) has a slightly lower apparent onset than that from (CO + LiOH) loss, but at high energies, the latter channel cross section dominates. This indicates that the loss of (CO + LiOH) must be entropically preferred compared to that for the loss of (CO + H_2O). Any mechanism describing the competition between these channels must therefore account for this observation.

3.2. Theoretical Results for Li^+(Pro) and Li^+(NMP) Reactants and Products

At all levels of theory, the ground conformer of Li^+(Pro) and Li^+(NMP) have been

established as zwitterionic [CO_2^-]C4-up,c structures [4,5], Figure 2. These are bidentate structures in which the lithium ion is coordinated to the carboxylate oxygens, designated by the notation in the square brackets, followed by the puckering position of the ring relative to the rest of the ring atoms and a designation of the ∠OCCN dihedral angle wherever needed to distinguish similar structures [4,5]. The four atoms in the ring with a dihedral angle closest to zero define the plane of the ring. The "out-of-plane" atom is designated "up" if it lies on the same side of the ring as the carboxylate group and "down" if it lies on the opposite side. The amine nitrogen is numbered 1, with the α-carbon being C2, and the remaining ring carbons are C3 through C5. (This naming scheme follows convention for the pyrrole ring and for proline, but differs from the nomenclature used in our previous papers where the α-carbon was C1 [4,5].) The ∠OCCN dihedral angle (where the O is the carbonyl oxygen that lies on the same side of the ring as N) is designated c for cis when the angle is less than 50°, g for gauche when the angle lies between 50° and 135°, and t for trans when the angle is greater than 135°.

In order to discuss the decomposition reactions observed experimentally in Figures 1, we need structures of the products, $C_4H_8N^+$ and $Li^+(C_4H_7N)$ from Li^+(Pro) and $C_5H_{10}N^+$ and $Li^+(C_5H_9N)$ from Li^+(NMP). Low-energy isomers for such products located at the MP2(full)/cc-pVDZ(Li-C) level along with their relative energies calculated at the MP2(full)/6-311+G(2d,2p)//B3LYP/6-311+G(d,p) level are shown in Figure 2. Table 1 lists the relative single point energies of the isomers of the two product ions. Values calculated using core correlation on Li^+ are comparable to those obtained by using standard basis sets for all the product ion isomers.

Several possible isomers of the $C_4H_8N^+$ product ion, formed by the loss of CO and LiOH from Li^+(Pro), were considered. These include H^+(2-pyrroline)[C3], H^+(3-pyrroline)[N], and H^+(2-pyrroline)[N] ions, which are abbreviated as H^+2Pyr[C3], H^+3Pyr[N], and H^+2Pyr[N]. Here, H^+ denotes the protonated species, which is followed by a number denoting the position of the double bond within the pyrroline ring, Pyr = pyrroline = c-C_4H_7N, and the position of the extra proton is indicated within square brackets. The lowest energy $C_4H_8N^+$ ion is H^+2Pyr[C3]

because it is stabilized by an imine double bond. The next two lowest energy product ions are H^+3Pyr[N] and H^+2Pyr[N], where the proton resides on the nitrogen. The former isomer of $C_4H_8N^+$ lies 39 – 48 kJ/mol above the ground isomer and the latter lies another 3 – 5 kJ/mol higher in energy.

A similar set of isomers exist for $Li^+(C_4H_7N)$ formed by loss of CO and H_2O from Li^+(Pro). Here, the lithium ion binding site is indicated within square brackets with the remaining nomenclature being the same as that of $C_4H_8N^+$. The lowest energy $Li^+(C_4H_7N)$ ion is Li^+1Pyr[N], with Li^+2Pyr[N] and Li^+3Pyr[N] lying significantly higher in energy, Table 1. For these two high energy isomers, the metal ion binding site is conserved but the C=C double bond is moved, leading to a difference in energy of 1 – 5 kJ/mol. The Li^+2Pyr[C3] isomer lies another 19 – 31 kJ/mol higher in energy because the carbon is a less favorable binding site for Li^+ compared to the nitrogen. We also located a species in which the lithium cation replaces the hydrogen atom on C2 (in essence, taking Li^+2Pyr[C3] and switching the C2 hydrogen and the lithium), as shown in the supplementary data, Figure S1. Because this species lies 95 – 108 kJ/mol above the ground Li^+1Pyr[N] ion, it will not be considered further.

Many of the possible isomers of $C_5H_{10}N^+$ formed by the loss of CO and LiOH from Li^+(NMP) directly parallel those for $C_4H_8N^+$, as shown in Figure 2, with the methyl group replacing the hydrogen on the nitrogen. These include H^+(1-methyl-2-pyrroline)[C3] or $H^+1CH_3$2Pyr[C3] along with $H^+1CH_3$3Pyr[N] and $H^+1CH_3$2Pyr[N]. In addition, the "extra" proton can move from the methyl group to a ring carbon yielding 1-methylene pyrrolidine cation or $1CH_2$pyrrolidine$^+$, where the ring is completely saturated because the imine double bond is outside the 5-membered ring. All levels of theory show that the lowest energy product ion formed by the loss of CO and LiOH is $H^+1CH_3$2Pyr[C3], in direct analogy to the lowest energy $C_4H_8N^+$ species. $1CH_2$pyrrolidine$^+$ is the next lowest energy isomer of $C_5H_{10}N^+$, lying 36 – 43 kJ/mol higher in energy. $H^+1CH_3$3Pyr[N] and $H^+1CH_3$2Pyr[N] have similar energies, lying 51 – 64 kJ/mol above the ground isomer.

The possible isomers of $Li^+(C_5H_9N)$ formed by the loss of (CO + H_2O) from Li^+(NMP)

are also directly analogous to the unmethylated versions and include $Li^+1CH_32Pyr[N]$, $Li^+1CH_33Pyr[N]$, and $Li^+1CH_32Pyr[C3]$. These three isomers have relative energies that parallel those found for $Li^+(C_4H_7N)$. The product ion directly analogous to $Li^+1Pyr[N]$ requires the migration of the methyl group to a ring carbon, which results in two more isomers. The first, $Li^+2CH_31Pyr[N]$, has the methyl group on C2 and is the ground $Li^+(C_4H_7N)$ structure. $Li^+3CH_31Pyr[N]$ has the methyl group on C3 and is calculated to lie 28 – 35 kJ/mol higher in energy. We also located additional $Li^+(C_5H_9N)$ isomers in which the lithium cation has replaced a hydrogen. Lithium can replace the hydrogen on C2, as for the analogous case of proline, or it can replace a hydrogen of the methyl group, as shown in the supplementary data, Figure S1. Again these isomers are quite high in energy, 136 – 145 and 172 – 183 kJ/mol, respectively, above the $Li^+2CH_31Pyr[N]$ ground isomer and are not considered further.

3.3. Pathway for CO loss from Li^+(Pro) and Li^+(NMP)

The complete mechanism for the loss of CO from Li^+(Pro) complexes computed at the MP2(full)/6-311+G(2d,2p)//B3LYP/6-311+G(d,p) level is shown in Figure S2 of the supplementary data with the relative single point energies of the TSs and intermediates listed in Table 2. Transition states are indicated by TS with a dash connecting changes in dihedral angle, metal ion coordination site, or backbone orientation. This nomenclature is adopted from that used in the study of protonated diglycine [34]. A detailed discussion of all the steps in this mechanism can be found in the supplementary data, while the present discussion focuses on only the key steps. Overall, the ground $[CO_2^-]$C4-up,c structure must transform into a charge-solvated [COOH]C3-down,t structure. This transformation requires a proton shift from the nitrogen to the carboxylate followed by rotation of the carboxylic acid group by 180° such that the N···H─OC hydrogen bond is broken. A concerted change in the puckering position of the ring also occurs and the lithium coordination changes from $[CO_2^-]$ to [CO] to [COOH]. The key step in this transformation is TS[CO]C(4-5)-up,(ct), which is 103 – 114 kJ/mol above the ground conformer. The charge-solvated Li^+(Pro) [COOH]C3-down,t structure, which lies 99 – 106 kJ/mol higher

UU IR Author Manuscript

than the ground $[CO_2^-]$C4-up,c isomer, can then decompose via TS[OH]{C2~CO~OH}, at the cost of 205 – 264 kJ/mol, Figures 3 and S2. In TS[OH]{C2~CO~OH}, the C2─CO and CO─OH bonds are synchronously broken (as indicated by the symbol ~ within curly brackets) resulting in the elimination of CO and formation of the proton bound intermediate, $(2Pyr[C3])H^+(LiOH_H)$, where the subscript indicates where the LiOH binds (in this case, to the proton through the oxygen). The product ion is characterized by a slightly elongated C3─H bond (1.15 Å as opposed to ~1.09 Å in the rest of the C─H bonds), an imine double bond (between N and C2), and an OH^- coordinated to Li^+. Theory indicates that the $(2Pyr[C3])H^+(LiOH_H)$ intermediate is 173 – 234 kJ/mol higher in energy than the ground reactant and lies 19 – 38 kJ/mol below the rate-limiting TS.

The complete PES including all TSs and intermediates involved in the loss of CO from Li^+(NMP) is directly analogous to that for Li^+(Pro) and thus is not shown here. The rate-limiting TS for elimination of CO lies 192 – 254 kJ/mol above the ground conformer of Li^+(NMP), $[CO_2^-]$C4-up,c. This leads to formation of an intermediate similar to the one obtained from Li^+(Pro), $(1CH_3 2Pyr[C3])H^+(LiOH_H)$, which lies 166 – 223 kJ/mol above the reactants. This TS is 10 – 14 kJ/mol lower than calculated for the Li^+(Pro) system, consistent with the observation that the apparent threshold for fragmentation decreases upon methylation. The initially formed intermediate from CO loss is 1 – 11 kJ/mol lower than the corresponding Li^+(Pro) species relative to their reactants.

3.4. Pathways for sequential loss of H_2O and LiOH from Li^+(Pro)

The $(2Pyr[C3])H^+(LiOH_H)$ intermediate is crucial to the decomposition of Li^+(Pro) because it can easily lose LiOH and rearrange to form an intermediate leading to loss of H_2O. Figure 3 shows these two pathways starting from TS[OH]{C2~CO~OH} with the relative energies of the corresponding intermediates, TSs, and products obtained from theory listed in Table 2.

Although $(2Pyr[C3])H^+(LiOH_H)$ can lose LiOH directly to form ground H^+2Pyr[C3]

products, it can also rearrange to a more stable intermediate by moving the coordination site of the LiOH moiety. The barrier associated with TS(H^+2Pyr[C3])($LiOH_{H\text{-}C2}$) is small, 0 – 6 kJ/mol above (2Pyr[C3])H^+($LiOH_H$). The resultant intermediate, H^+2Pyr[C3]C4-down($LiOH_{C2}$) is stabilized by a H-bond between N and the LiOH hydrogen of 2.20 Å. (Note that the presence of the LiOH has distorted the ring inducing a pucker, which we now specify with down meaning the C4 carbon is directed to the opposite side of the ring from the LiOH.) H^+2Pyr[C3]C4-down($LiOH_{C2}$) is 15 – 47 kJ/mol lower in energy than (2Pyr[C3])H^+($LiOH_H$). At the cost of 3 – 7 kJ/mol, the pucker of the pyrroline ring changes from C4-down to C4-up to form H^+2Pyr[C3]C4-up($LiOH_{C2}$). This intermediate can then go over a barrier, TS(H^+2Pyr[C3])($LiOH_{C2\text{-}NH}$), which involves moving the LiOH moiety away from the ring structure to form a hydrogen bond at the nitrogen. The resultant complex H^+2Pyr[C3]($LiOH_{NH}$) has two stable forms with Li^+ on opposite sides of the plane of the ring. These differ by less than 0.2 kJ/mol and are separated by a TS lying 3.3 – 3.8 kJ/mol higher (not shown). From any of these intermediates, loss of LiOH can occur over a loose transition state to form the products, H^+2Pyr[C3] + LiOH. The products lie 250 – 319 kJ/mol above the ground reactants and 45 – 67 kJ/mol above the rate-limiting TS for CO loss.

For the competing channel, loss of H_2O, the metal ion in H^+2Pyr[C3]($LiOH_{NH}$) reorients such that it binds to the ring nitrogen. This change in the metal co-ordination costs 13 – 17 kJ/mol of energy and results in the formation of (1Pyr[N])Li^+(H_2O), which lies 39 – 90 kJ/mol above Li^+(Pro). Here, the Li^+ bridges the pyrroline and water ligands and loss of water can occur over a loose TS to form Li^+1Pyr[N], 149 – 200 kJ/mol above reactants and 43 – 78 kJ/mol below the rate-limiting TS for CO loss. In our search for the lowest energy pathway, we also located another pathway for the loss of water that involves rearrangement of the initially formed (2Pyr[C3])H^+($LiOH_H$) intermediate, but this pathway results in the formation of the Li^+2Pyr[N] isomer of Li^+(C_4H_7N), 54 – 58 kJ/mol higher in energy. Details of this pathway can be found in the supplementary data.

Overall, the loss of CO is limited by the tight transition state, TS[OH]{C2~CO~OH},

UU IR Author Manuscript

which also limits the subsequent loss of H_2O. The further loss of LiOH is limited by the energy of the products, H^+2Pyr[C3] + LiOH. Because loss of H_2O can occur rapidly once CO loss is energetically possible, the CO loss product is not observed experimentally. Clearly, the loss of water is lower in energy than loss of LiOH, in agreement with experiment. Also the rate-limiting tight TS for CO loss forms a species having the LiOH moiety, such that loss of LiOH should be entropically more favorable, again in agreement with the preferred formation of LiOH at higher energies, Figure 1a.

3.5. Pathways for sequential loss of H_2O and LiOH from Li^+(NMP)

The mechanism for loss of LiOH from Li^+(NMP), Figure 4, differs somewhat from that of Li^+(Pro). Table 3 lists the relative energies of the intermediates, TSs, and products of Li^+(NMP) fragmentation as obtained from theory. From ($1CH_3$2Pyr[C3])H^+($LiOH_H$), the system passes over TS($H^+1CH_3$2Pyr[C3])($LiOH_{H\text{-}C2}$), which lies 164 – 228 kJ/mol above ground Li^+(NMP), and leads to $H^+1CH_3$2Pyr[C3]($LiOH_{C2}$), lying 9 – 19 kJ/mol lower than the TS (9 kJ/mol above at the B3LYP/aug-cc-pVTZ(Li─C) level). This TS and intermediate are directly analogous to those of the Li^+(Pro) system, however, the next steps differ because methylation of the nitrogen prevents the LiOH from moving to form a hydrogen bond at NH and further keeps the 5-membered ring relatively flat such that there are no conformers differing in the pucker of the ring. Thus, the LiOH moiety moves over a small barrier from C2 to the C2 hydrogen to form $H^+1CH_3$2Pyr[C3]($LiOH_{C2H}$), such that LiOH lies in a bridging position between C2H, r(C2H-O) = 1.83 Å, and the methyl group, r(CH-O) = 2.44 Å. $H^+1CH_3$2Pyr[C3]($LiOH_{C2H}$) lies 148 – 209 kJ/mol above the ground reactants and 51 – 68 kJ/mol higher than the H^+2Pyr[C3]($LiOH_{NH}$) intermediate for Li^+(Pro). Formation of products, $H^+1CH_3$2Pyr[C3] + LiOH, can occur from any of these $H^+1CH_3$2Pyr[C3](LiOH) intermediates over a loose transition state lying 230 – 306 kJ/mol above the ground reactants and 36 – 60 kJ/mol above the rate-limiting TS for elimination of CO.

The mechanism for loss of water from Li^+(NMP) differs from that of Li^+(Pro), again

UU IR Author Manuscript

because the nitrogen is methylated. Beginning with ($1CH_32Pyr[C3])H^+(LiOH_H$), the shared proton shifts towards the oxygen of LiOH passing over $TS(1CH_32Pyr)H^+_{C3\text{-}OH}$(LiOH) and forming $(1CH_32Pyr_H)(H_2O)Li^+$. All levels of theory but MP2(full) predict this intermediate to be unstable once zero point energies are included. The next TS, $TS(1CH_32Pyr_{H\text{-}Li})Li^+(H_2O)$, moves the coordination of Li^+ to the nitrogen, which requires 7 – 10 kJ/mol and forms $(1CH_32Pyr[N])Li^+(H_2O)$, which lies 108 – 157 kJ/mol above ground Li^+(NMP). This intermediate is the most stable species formed after decarbonylation of Li^+(NMP) and leads to the products, $Li^+1CH_32Pyr[N] + H_2O$ via a loose TS. These products are 215 – 267 kJ/mol above the ground reactants and 12 – 32 kJ/mol above the rate-limiting TS for CO loss at all levels of theory except for the MP2(full)/6-311+G(2d,2p) level, where it is 0.6 kJ/mol lower. The product ion formed from water loss is not the lowest energy isomer, $Li^+2CH_31Pyr[N]$, but formation of this isomer requires the methyl group to migrate to the C2 ring carbon. We find that the barrier for such a transformation lies 505 – 546 kJ/mol above ground Li^+(NMP) indicating that the formation of $Li^+2CH_31Pyr[N]$ is unlikely. Alternatively, $(1CH_32Pyr[N])Li^+(H_2O)$ can lose pyrroline over a loose transition state to form $Li^+(H_2O)$, 244 – 325 kJ/mol above the ground reactants and 29 – 67 above the $Li^+1CH_32Pyr[N] + H_2O$ products.

Analogous to the Li^+(Pro) fragmentation, the loss of CO from Li^+(NMP) is limited by the tight transition state, TS[OH]{C2~CO~OH}, at all levels of theory. The rate-limiting TS for LiOH loss is found to be loose at all levels of theory, and the same is true for H_2O loss except for the MP2(full)/6-311+G(2d,2p) level of theory where it is limited by the tight TS for CO loss. At all levels of theory, the energy required for loss of water is close (-0.6 – 32 kJ/mol) to the TS for loss of CO, which agrees with our experimental observation that loss of CO alone is not observed. The $Li^+1CH_32Pyr[N] + H_2O$ products are calculated to lie lower in energy than $H^+1CH_32Pyr[C3])$ + LiOH products, consistent with our experimental data. Like in Li^+(Pro), the rate-limiting tight TS for CO loss forms a species having the LiOH moiety, such that loss of LiOH is entropically favorable, again in agreement with the preferred formation of LiOH at higher energies, Figure 1b.

UU IR Author Manuscript

4. Data Analysis

The experimental results show that the decompositions involving the loss of (CO + H_2O/LiOH) are the lowest energy processes for both Li^+(Pro) and Li^+(NMP). Figures 1a and 1b clearly show the competition between these two low-energy reactions. In addition, in the Li^+(Pro) system, the formation of Li^+ is dominant at high energies, indicating that it is an entropically favored process, even though it has the highest threshold energy. Thus, the cross sections for (CO + H_2O) and (CO + LiOH) loss decrease as the cross section for Li^+ formation increases, indicating that the formation of Li^+ is competing with the loss of CO. The same competition is not obvious for the Li^+(NMP) system because the Li^+ channel cross section is much smaller. Theory would suggest this occurs because the CO loss channel now has a lower energy transition state whereas the binding energy of Li^+ to NMP is slightly higher, such that formation of Li^+ + NMP is limited by competition. Indeed, for the other alkali metal cations, Na^+, K^+, and Rb^+, NMP binds more strongly than Pro by ~ 8 kJ/mol [5].

4.1. Threshold Analysis for Li^+(Pro)

When the Li^+ product obtained from the CID of Li^+(Pro) is analyzed independently using a PSL TS, a threshold energy of 2.80 ± 0.09 eV is obtained, Table 4. This product exhibits a fairly large kinetic shift of 0.81 eV in part because of the relatively high threshold. The PSL threshold measured here agrees with the previously published threshold energy of 2.89 ± 0.10 eV [4]. We also independently analyze the cross section for the competing channel, loss of CO, where the CO loss cross section is represented by summing the cross sections for the Li^+1Pyr[N] + CO + H_2O and H^+2Pyr[C3] + CO + LiOH product channels. Because the primary ion formed from the loss of CO was not observed experimentally, this model assumes that the intermediate formed by CO loss can rapidly dissociate further by water loss with no additional energy needed, as found computationally, Figure 3. Thus the rate-limiting TS for the cross section sum is assigned to the tight TS for CO loss, TS[OH]{C2~CO~OH}. Here the threshold for CO loss is

2.51 ± 0.14 eV.

These independent analyses ignore the competition between the two primary reactions, which we now model using the tight TS for CO loss and a loose PSL TS for Li^+ + Pro formation. In this analysis (not included in Table 4), the relative scaling constants for the two channels $\sigma_{0,j}$ are on the order of 10^6, for which there is no adequate physical explanation. Previously [46,47], we have accounted for such large scaling factors by adjusting the relative tightness of the competing TSs. As the loose PSL TS is already the loosest possible, comparable $\sigma_{0,j}$ values for the two channels are obtained when the low frequency modes (below 1000 cm^{-1}) of TS[OH]{C2~CO~OH} are tightened by a factor of 2 ± 0.2. (In this regard, it may be useful to note that the Gaussian software issues a warning that the thermodynamic functions may be erroneous for vibrational frequencies under 625 cm^{-1} ≡ 900 K, because such vibrations cannot be treated accurately as harmonic at temperatures of interest.) This competitive analysis is shown in Figure 5a and can be seen to reproduce the experimental data including the competition over broad ranges of energy (~4 eV) and cross section magnitude (> two orders of magnitude). This analysis yields thresholds of 2.06 ± 0.09 eV for the cross section sum and 2.67 ± 0.05 eV for Li^+, Table 4. The model does not reproduce either cross section at energies greater than ~5 eV because it does not include the possibility that the Li^+1Pyr[N] product can decompose at these high energies and contribute to the Li^+ product. In this regard, we note that the discrepancies between the models and cross sections are comparable in magnitude and opposite in sign, ~0.5 × 10^{-16} cm^2, consistent with this sequential reaction. At present, this particular process cannot be directly modeled because the CRUNCH program [48] used for data analysis is not capable of treating systems that dissociate beyond two sequential steps, i.e., dissociation to a total of four or more products. Note that the threshold for CO loss has decreased by 0.45 eV because the kinetic shift is much larger for the TS with tightened frequencies ($\Delta S^{\ddagger}$ value of -39 J/mol K compared to 82 J/mol K for the TS without scaling frequencies). The threshold for Li^+ formation has also decreased by 0.13 eV as a result of accounting for the competition with the low energy channels. This competitive shift is comparable to those observed for fragmentations of Li^+(Met), Li^+(Ser),

and Li^+(Thr) [43,44].

Having successfully modeled the two primary reactions, we next analyze the competition between the two low-energy sequential fragmentations, initially without accounting for the Li^+ channel. Here, the formation of Li^+1Pyr[N] + CO + H_2O products is limited by the tight TS for CO loss (again with frequencies below 1000 cm^{-1} scaled by 2), whereas the loss of LiOH is analyzed as a sequential dissociation via a loose PSL TS after the loss of CO, as suggested by the potential energy surface of Figure 3. Analysis of these cross sections up to 4.5 eV yields thresholds of 1.96 ± 0.07 eV for CO loss and 2.84 ± 0.05 eV for subsequent LiOH loss, Table 4. The model does not reproduce the cross sections at energies greater than 4.5 eV primarily because the possibility that the Li^+1Pyr[N] product decomposes to contribute to the Li^+ product at these high energies is not included in this model. As noted above, because of the kinetic energy release that might occur once past TS[OH]{C2~CO~OH}, the sequential threshold for LiOH loss may be inaccurate and is conservatively viewed as an upper limit.

Finally, we modeled all three fragmentations simultaneously, as shown in Figure 5b, where the frequencies below 1000 cm^{-1} for the tight TS for CO loss were scaled by a factor of 2 ± 0.2. The thresholds obtained are 2.05 ± 0.07 eV for the lowest energy decomposition (CO + H_2O loss), <2.86 ± 0.12 eV for (CO + LiOH) loss, and 2.64 ± 0.07 eV for Li^+ formation, Table 4, and are believed to be our best overall model although the kinetic shift for the CO loss may be overestimated. These thresholds agree with those obtained from the competitive fit shown in Figure 5a, whereas those for the two low-lying channels are slightly higher than those from the simpler model.

As shown in Table 4, the activation entropies at 1000 K, $\Delta S^{\dagger}_{1000}$, of the three reactions as obtained from the analysis of the experimental data are -39 J/mol K for the tight CO loss TS, which also limits formation of Li^+1Pyr[N] + CO + H_2O, -7 J/mol K for the formation of H^+2Pyr[C3] + CO + LiOH, and 43 J/mol K for Li^+ + Pro. These $\Delta S^{\dagger}_{1000}$ values are characteristic of the TSs involved in the fragmentation. The differences in the values of $\Delta S^{\dagger}_{1000}$ for water loss and LiOH loss reflect the different TSs used for modeling the two decompositions. These TSs

UU IR Author Manuscript

are particularly tight because of the frequency scaling needed to account for the competition between the low energy channels and the loss of Pro. The $\Delta S^{\ddagger}_{1000}$ value for the loose PSL TS leading to Li^+ + Pro lies in the range determined by Lifshitz for simple bond cleavages [49].

4.2. Threshold Analysis for Li^+(NMP)

We begin the data analysis by fitting the Li^+ product cross section independently, which gives a threshold of 3.39 ± 0.17 eV, Table 4. For reasons discussed in our previous study of M^+(NMP) complexes [5], the analysis of the Li^+ + NMP channel treats the methyl group in the NMP ligand as an internal rotor, i.e., the methyl torsional vibration of 228 cm^{-1} is replaced by an internal rotational constant of 5.4 cm^{-1} [50]. Note that this threshold energy is well above those obtained for the analogous channel in the Li^+(Pro) system. This result appears to be primarily a consequence of not accounting for the competition with the other primary fragmentation, CO loss, which is much more severe than in the Li^+(Pro) system. Independent analysis of the low energy channels, again performed as the sum of the (CO + H_2O) and (CO + LiOH) loss channels, yields a threshold of 2.56 ± 0.06 eV, very similar to that obtained for Li^+(Pro) when the CO loss TS frequencies are unscaled.

We also model the experimental data to include the competition between the primary channels of CO loss and Li^+ formation as well as the competition between the two low-energy sequential decompositions occurring after CO loss. Competition between the loss of CO over a tight TS and formation of Li^+ over a loose PSL TS can be modeled with reasonable $\sigma_{0,j}$ scaling factors if the tight CO loss TS frequencies below 1000 cm^{-1} are scaled by a factor of 1.26 ± 0.02. Accurate reproduction of the shape of the cross section sum at the higher energies where the Li^+ product is formed necessitates a small value (~0.8) of the *n* parameter in Eq. (1). Such a competitive fit, shown in Figure 5c, gives thresholds of 2.63 ± 0.11 eV for the cross section sum and 3.45 ± 0.11 eV for Li^+ formation. Notably, this model does not include the possibility that the $Li^+1CH_32Pyr[N]$ product formed by loss of (CO + H_2O) can also dissociate and contribute to Li^+ formation. This third order process cannot be modeled using the present program, as noted

UU IR Author Manuscript

above. Although it is feasible that this process could account for much of the Li^+ product formed, our quantum chemical results indicate that this channel does not open until 4.0 – 4.4 eV, Table 3, well above the measured threshold.

Competition between the two low-energy decompositions of Li^+(NMP) were analyzed in three different ways to determine the best approach for reproducing the experimental data. The three models are classified based on the TSs designated for CO loss, water loss, and LiOH loss, namely tight-loose-loose (TLL), tight-tight-loose (TTL), and tight-loose (TL) model. In the TL model, the TSs for the CO loss and subsequent water loss channels are merged, the same approach used for Li^+(Pro). Of the three models, the best reproduction of the experimental cross sections for the low-energy fragmentations of Li^+(NMP) is provided by the TL model, which is discussed further here. More detailed results from other two models (TLL and TTL) can be found in the supplementary data but in both cases, these models predict that the product formed by CO loss should have an appreciable cross section, in contrast to observation. In the TL model, the tight TS for CO loss limits the subsequent water loss, such that no CO loss product should be observed, and the loss of LiOH is limited by a loose TS. Such a competitive fit is shown in Figure 5d and furnishes thresholds of 2.34 ± 0.05 eV for CO and subsequent water loss and <3.07 ± 0.10 eV for LiOH loss when the CO loss TS frequencies are scaled by 1.26 ± 0.02. (Thresholds are 2.58 ± 0.07 and <3.07 ± 0.11 eV, respectively, if no frequency scaling is employed, Table 4.) The TL model (as well as the TLL and TTL models) does not reproduce the sequential processes above ~5 eV, Figure 5d, because accurate reproduction of the data above 5 eV requires a different value of *n* to reproduce the shape of the total experimental cross sections at high energies and subsequent decomposition of the $Li^+1CH_32Pyr[N]$ product is not included.

As noted above, the competitive shift observed in the Li^+(Pro) system is about 0.14 eV, consistent with previous results for similarly sized systems [43,44]. In the case of Li^+(NMP), analysis of the Li^+ cross section with and without including competition with CO loss gives the same threshold energy of ~3.4 eV, but utilizes very different *n* values. To obtain an accurate estimate of the competitive shift, we independently analyze the Li^+ cross section using the small

n value (0.8, Table 4). The threshold of 4.10 eV is 0.71 ± 0.08 eV higher than that obtained using the competitive model and the small *n* value. Subtracting this difference from the Li^+ threshold energy obtained from the competitive model gives E_0 = 2.74 ± 0.14 eV, which we believe is our best threshold energy for the Li^+ product.

5. Discussion

5.1. Comparison of Theoretical and Experimental Thermochemistry: Products

Experimental threshold energies are compared with energies of the product ions calculated at different levels of theory in Table 5. For Li^+(Pro), the sequential and competitive analysis of all three fragmentations as shown in Figure 5b gives our best threshold energies, although the large frequency scaling factor needed to account for the competition (2 ± 0.2) leads to a large kinetic shift that might be overestimated. Because theory shows that the experimental threshold energy for Li^+1Pyr[N] + CO + H_2O is limited by the tight TS for CO loss, TS[OH]{C2~CO~OH}, this experimental value is compared to the theoretical value for this TS. All three levels of theory predict Li^+–Pro BDEs that are comparable to the experimental value, with B3LYP being slightly high. In contrast, B3LYP gives reasonable agreement with the experimental threshold energy for CO loss, whereas B3P86 and MP2 approaches are high by 40 – 66 kJ/mol, consistent with an overestimated kinetic shift. For the fragmentation to H^+2Pyr[C3] + CO + LiOH, the measured threshold is predicted reasonably well by the MP2/6-311+G(2d,2p) approach with B3LYP being low and B3P86 being high. Calculations also find that this threshold lies 41 – 67 kJ/mol above the CO loss TS, whereas the experimental difference is <78 ± 14 kJ/mol. This comparison is consistent with the threshold for the (CO + LiOH) channel determined using the statistical sequential model being only an upper limit or with the kinetic shift associated with the CO loss TS being overestimated.

For the Li^+(NMP) system, we again compare the experimental threshold energy for the loss of (CO + H_2O) to that obtained from theory for the rate-limiting CO loss TS. As noted above, the frequency scaling factor needed to model the data without scaling the cross sections is

UU IR Author Manuscript

1.26 ± 0.02. This modest change is reasonable, such that the kinetic shift is more likely to be estimated accurately. Although most levels of theory predict that the loss of water from Li^+(NMP) is loose, modeling the data using this assumption predicts that the product formed by loss of CO should be observed. Thus, our best model of the data utilizes the TL approach, which parallels that taken for Li^+(Pro) and is consistent with the MP2/6-311+G(2d,2p) results. We find that the threshold energy for CO loss agrees best with the values predicted by the B3P86 and MP2 levels of theory. Calculations suggest that the difference in threshold energies between the loss of CO and (CO + LiOH) is 36 – 60 kJ/mol, compared to an experimental value of <70 ± 11 kJ/mol. When the Li^+ + NMP bond energy of 264 ± 13 kJ/mol (estimated as detailed above) is compared with theory, we find that MP2(full)/6-311+G(2d,2p) results give the best agreement with experiment, although both B3LYP and B3P86 approaches are only slightly higher.

When the four experimental threshold energies for the Li^+(Pro) and Li^+(NMP) systems are compared with theory (excluding the LiOH product channels because they are upper limits), B3P86 and MP2(full))/6-311+G(2d,2p) approaches give the lowest MADs of ~14 kJ/mol with that for B3LYP being only slightly higher, 18 kJ/mol, Table 5. The MP2(full)/aug-cc-pVTZ(Li-C) approach is appreciably worse (MAD = 29 kJ/mol) because it overestimates the TS energies. If the LiOH product channels are included, the B3P86 and MP2(full)/6-311+G(2d,2p) results keep MADs of ~16 kJ/mol, whereas the B3LYP comparison rises to about 26 kJ/mol. Overall, the MP2(full)/6-311+G(2d,2p) approach leads to the best agreement between theory and experiment, not only in terms of the exact values, but the observation that the TS for CO loss limits the formation of the (CO + H_2O) product channel. The only significant deviation occurs for the TS for CO loss in the Li^+(Pro) system, which strongly suggests that the kinetic shift in this channel is overestimated as a result of the large frequency scaling factor needed to reproduce the competition between the CO loss and Li^+ + Pro channels.

5.2. Side-Chain Effects

In our previous study of the CID of M^+(NMP), the bond energy of Li^+ to Pro was

reported to increase by 8 kJ/mol upon methylation of proline [5]. There the comparison was made to a Li^+-Pro experimental bond energy of 279 ± 10 kJ/mol, which was obtained by independent analyses excluding competition with the other primary fragmentation, loss of CO [4]. Including the competition with CO results in lowering the Li^+ + Pro bond energy by 24 ± 12 kJ/mol. Also the Li^+ threshold energy from Li^+(NMP) obtained in a previous study was obtained using the TLL model to analyze the competition of Li^+ with the loss of CO. Here, we find that the analysis of the low-energy fragmentations from Li^+(NMP) using the TL method reproduces the cross sections of (CO + H_2O) loss and (CO + LiOH) loss in accord with our assumptions. According to the bond energies in Table 5, the binding energy of Li^+ increases by 9 ± 15 kJ/mol upon methylation. This difference is in agreement with the previous study [5] and with theory, which predicts an increase of 8 – 15 kJ/mol. This increase in the Li^+ binding energy upon methylation also agrees with increases measured for similar methylated systems studied previously [5,44,51-53].

Replacement of a H with CH_3 on the nitrogen of lithiated proline has a significant effect on the thresholds of both low-energy fragmentations. The threshold energy for CO loss from lithiated proline increases by 28 ± 9 kJ/mol upon methylation, whereas calculations predict a decrease of 10 – 14 kJ/mol, with the MP2 approach showing the smallest differences. However, as noted above, it seems likely that the kinetic shift for CO loss in the Li^+(Pro) system is overestimated, such that the true threshold for CO loss is probably higher. A more accurate estimate of the effect of methylation on this channel therefore comes from comparing the threshold analysis for the low energy decompositions without frequency scaling. The most accurate value probably comes from analysis of the summed cross sections, Table 4, in which case the difference is 5 ± 14 kJ/mol, comparable to theory. Likewise, the threshold energies for (CO + LiOH) loss are somewhat higher for Li^+(NMP) compared to Li^+(Pro), with theory predicting a decrease of 14 – 20 kJ/mol upon methylation.

UU IR Author Manuscript

6. Conclusions

In addition to the loss of the amino acid ligand, elimination of (CO + H_2O) and (CO + LiOH) were observed in the CID of Li^+(Pro) and Li^+(NMP) at low energies. Examination of the potential energy surface for these fragmentations reveals that the loss of CO is followed by a sequential loss of water and LiOH, where water loss is limited by the tight transition state for initial CO loss (although not at all levels of theory for NMP) and LiOH loss is limited by its asymptotic loose TS. The experimental data show that the loss of water is energetically favored while loss of LiOH is entropically favored, which is consistent with the reaction mechanisms found for these decompositions in both systems. We find that the cross sections for (CO + H_2O) and (CO + LiOH) loss decrease as the cross section of Li^+ formation increases in the Li^+(Pro) system, indicating that the formation of Li^+ is competing with the loss of CO. For Li^+(NMP), such competition is not evident because the low energy pathways are lower in energy and loss of NMP is higher. Analysis of these reaction cross sections requires modeling the competition of Li^+ formation with the CO loss and including a subsequent dissociation to water and LiOH. Such an analysis allows us to extract threshold energies for decarbonylation and the bond energy of Li^+ + Pro and NMP. This study refines the bond energy of Li^+ to Pro obtained previously by Moision and Armentrout [4] by including the competition with the other primary reaction channel, which lowers the previous value by 24 ± 12 kJ/mol. The present evaluation of the bond energy of Li^+ to NMP is found to be 9 ± 15 kJ/mol higher than to Pro, consistent with previous determinations of how methylation can affect metal-ligand bond energies [5,44,51-53]. Comparison with theory suggests that MP2(full)/6-311G+(2d,2p) yields the best results for both Li^+(Pro) and Li^+(NMP) because these computations agree best with experimental thresholds and are consistent with the assumptions needed to model the data accurately.

Acknowledgement

This work is supported by the National Science Foundation, grant CHE-1049580, and DBI-0922819 for acquisition of the FTICR instrument. The authors also acknowledge the Centre for High Performance Computing (CHPC), University of Utah for granting generous computer time. C. He and Prof. M. T. Rodgers are thanked for performing the high mass accuracy experiments in the FTICR.

Appendix A. Supplementary Data

CID cross sections of all products observed in Li^+(NMP) decomposition are shown in Figure S1. Exact mass measurements done using FTICR on Li^+(Pro) and its SORI-CAD spectrum are in Figure S2. Figure S3 shows the SORI-CAD spectrum of the m/z 104 product ion formed from Li^+(Pro). The high energy isomers of the product ion formed by loss of ($CO + H_2O$) from Li^+(Pro) and Li^+(NMP) are shown in Figure S4. Details of the decarbonylation reaction mechanism are discussed and shown in Figure S5. An alternative pathway for the loss of water from Li^+(Pro) is discussed and shown in Figure S6. Detailed discussion of the competitive analysis of the low-energy decompositions using the TLL and TTL models for Li^+(NMP). The fitting parameters from the two models are listed in Table S1 and the fit obtained from the TTL model is shown in Figure S7.

UU IR Author Manuscript

UU IR Author Manuscript

References

[1] J.A. Ibers, R.H. Holm, Science 209 (1980) 223.
[2] J.M. Castagnetto, S.W. Hennessy, V.A. Roberts, E.D. Getzoff, J.A. Tainer, M.E. Pique, Nucl. Acids. Res. 30 (2002) 379.
[3] T.-Y. Kim, S.J. Valentine, D.E. Clemmer, J.P. Reilly, J. Am. Mass. Spectrom. 21 (2010) 1455.
[4] R.M. Moision, P.B. Armentrout, J. Phys. Chem. A 110 (2006) 3933.
[5] A. Mookherjee, P.B. Armentrout, Int. J. Mass Spectrom. 345-347 (2013) 109.
[6] R.B. Cody Jr., I.J. Amster, F.W. McLafferty, Proc. Natl. Acad. Sci. USA 82 (1985) 6367.
[7] T. Lin, G.L. Glish, Anal. Chem. 70 (1998) 5162.
[8] S.-W. Lee, H.S. Kim, J.L. Beauchamp, J. Am. Chem. Soc. 120 (1998) 3188.
[9] L.M. Teesch, J. Adams, Organic Mass Spectrom. 27 (1992) 931.
[10] X. Tang, W. Ens, K.G. Standing, J.B. Westmore, Anal. Chem. 60 (1988) 1791.
[11] D. Renner, G. Spiteller, Biomed. Environ. Mass Spectrom. 15 (1988) 75.
[12] J.J. Russell, J.A. Seetula, D. Gutman, J. Am. Chem. Soc. 110 (1988) 3092.
[13] R.P. Grese, R.L. Cerny, M.L. Gross, J. Am. Chem. Soc. 111 (1989) 2835.
[14] R.P. Grese, M.L. Gross, J. Am. Chem. Soc. 112 (1990) 5098.
[15] M.M. Kish, C. Wesdemiotis, Int. J. Mass Spectrom. 227 (2003) 191.
[16] F. Muntean, P.B. Armentrout, J. Chem. Phys. 115 (2001) 1213.
[17] K.M. Ervin, P.B. Armentrout, J. Chem. Phys. 83 (1985) 166.
[18] M.T. Rodgers, K.M. Ervin, P.B. Armentrout, J. Chem. Phys. 106 (1997) 4499.
[19] M.T. Rodgers, P.B. Armentrout, J. Chem. Phys. 109 (1998) 1787.
[20] T.S. Beyer, D.F. Swinehart, Commun. ACM 16 (1973) 379.
[21] S.E. Stein, B.S. Rabinovich, Chem. Phys. Lett. 49 (1977) 183.
[22] R.G. Gilbert, S.C. Smith, Theory of Unimolecular and Recombination Reactions, Blackwell Scientific, London, 1990.
[23] K.A. Holbrook, M.J. Pilling, S.H. Robertson, Unimolecular Reactions, Wiley, New York, 1996.
[24] P.B. Armentrout, J. Chem. Phys. 126 (2007) 234302.
[25] D.A. Hales, L. Lian, P.B. Armentrout, Int. J. Mass Spectrom. Ion Processes 102 (1990) 269.
[26] P.J. Chantry, J. Chem. Phys. 55 (1971) 2746.
[27] C. Lifshitz, R.L.C. Wu, T.O. Tiernan, D.T. Terwilliger, J. Chem. Phys. 68 (1978) 247.
[28] M.J. Frisch, G.W. Trucks, H.B. Schlegel, G.E. Scuseria, M.A. Robb, J.R. Cheeseman, G. Scalmani, V. Barone, B. Mennucci, G.A. Petersson, H. Nakatsuji, M. Caricato, X. Li, H.P. Hratchian, A.F. Izmaylov, J. Bloino, G. Zheng, J.L. Sonnenberg, M. Hada, M. Ehara, K. Toyota, R. Fukuda, J. Hasegawa, M. Ishida, T. Nakajima, Y. Honda, O. Kitao, H. Nakai, T. Vreven, J.A. Montgomery, J.E. Peralta, F. Ogliaro, M. Bearpark, J.J. Heyd, E. Brothers, K.N. Kudin, V.N. Staroverov, R. Kobayashi, J. Normand, K. Raghavachari, A. Rendell, J.C. Burant, J.M. Millam, S.S. Iyengar, J. Tomasi, M. Cossi, N. Rega, J.M. Millam, M. Klene, J.E. Knox, J.B. Cross, V. Bakken, C. Adamo, J. Jaramillo, R. Gomperts, R.E. Stratmann, O. Yazyev, A.J. Austin, R. Cammi, C. Pomelli, J.W. Ochterski, R.L. Martin, K. Morokuma, V.G. Zakrzewski, G.A. Voth, P. Salvador, J.J. Dannenberg, S. Dapprich, A.D. Daniels, O. Farkas, J.B. Foresman, J.V. Ortiz, J. Cioslowski, D.J. Fox, Gaussian 09, Revision A.02. Gaussian Inc., Pittsburgh, PA, 2009.
[29] C.Y. Peng, H.B. Schlegel, Israel J. Chem. 33 (1994) 449.

[30] C.Y. Peng, P.Y. Ayala, H.B. Schlegel, M.J. Frisch, J. Comp. Chem. 17 (1996) 49.
[31] R.M. Moision, P.B. Armentrout, J. Phys. Chem. A 106 (2002) 10350.
[32] R.M. Moision, P.B. Armentrout, Phys. Chem. Chem. Phys. 6 (2004) 2588.
[33] S.J. Ye, P.B. Armentrout, J. Phys. Chem. A 112 (2008) 3587.
[34] P.B. Armentrout, A.L. Heaton, J. Am. Soc. Mass Spectrom. 23 (2012) 621.
[35] P.B. Armentrout, A.L. Heaton, S.J. Ye, J. Phys. Chem. A 115 (2011) 11144.
[36] J.B. Foresman, A.E. Frisch, Exploring Chemistry with Electronic Structure Methods, Gaussian, Inc., Pittsburgh, PA, 1996.
[37] F.B. van Duijneveldt, J.G.C.M. van Duijneveldt-van de Rijdt, J.H. van Lenthe, Chem. Rev. 94 (1994) 1873.
[38] M.T. Rodgers, P.B. Armentrout, Int. J. Mass Spectrom. 267 (2007) 167.
[39] T.H. Dunning, J. Chem. Phys. 90 (1989) 1007.
[40] R.A. Kendall, T.H. Dunning, R.J. Harrison, J. Chem. Phys. 96 (1992) 6796.
[41] C. Guo, Y. Zhou, P. Liu, Y. Chai, Y. Pan, J. Am. Soc. Mass Spectrom. 23 (2012) 1191.
[42] M.T. Rodgers, P.B. Armentrout, J. Phys. Chem. A 101 (1997) 2614.
[43] P.B. Armentrout, A. Gabriel, R.M. Moision, Int. J. Mass Spectrom. 283 (2009) 56.
[44] S.J. Ye, P.B. Armentrout, J. Phys. Chem. B 112 (2008) 10303.
[45] P.B. Armentrout, S.J. Ye, A. Gabriel, R.M. Moision, J. Phys. Chem. B 114 (2010) 3938.
[46] A.L. Heaton, P.B. Armentrout, J. Am. Soc. Mass Spectrom. 20 (2009) 852.
[47] P.B. Armentrout, E.M.S. Stennett, J. Am. Soc. Mass Spectrom. 25 (2014) 512.
[48] P.B. Armentrout, K.M. Ervin, M.T. Rodgers, J. Phys. Chem. A 112 (2008) 10071.
[49] C. Lifshitz, Adv. Mass Spectrom. 11 (1989) 713.
[50] L.H. Sprangler, Annu. Rev. Phys. Chem. 48 (1997) 475.
[51] V.N. Bowman, A.L. Heaton, P.B. Armentrout, J. Phys. Chem. B 114 (2010) 4107.
[52] N. Hallowita, D.R. Carl, P.B. Armentrout, M.T. Rodgers, J. Phys. Chem. A 112 (2008) 7996.
[53] R. Amunugama, M.T. Rodgers, Int. J. Mass Spectrom. 227 (2003) 339.

UU IR Author Manuscript

Table 1. Relative energies (kJ/mol) of the isomers of fragment ions obtained from Li^+(Pro) and Li^+(NMP) decomposition.

product ion	structure	theory[a]		
		B3LYP	B3P86	MP2(full)
$C_4H_8N^+$	H^+2Pyr[C3]	0.0, *0.0*	0.0, *0.0*	0.0, *0.0*
	H^+3Pyr[N]	46.9, *47.8*	47.8, *48.2*	41.1, *39.4*
	H^+2Pyr[N]	51.2, *51.7*	51.5, *51.6*	46.5, *44.7*
$Li^+(C_4H_7N)$	Li^+1Pyr[N]	0.0, *0.0*	0.0, *0.0*	0.0, *0.0*
	Li^+2Pyr[N]	58.2, *57.4*	56.1, *54.4*	56.3, *54.3*
	Li^+3Pyr[N]	63.0, *62.4*	60.0, *58.5*	57.6, *56.6*
	Li^+2Pyr[C3]	83.6, *81.4*	79.5, *77.7*	88.9, *87.4*
$C_5H_{10}N^+$	H^+1$CH_3$2Pyr[C3]	0.0, *0.0*	0.0, *0.0*	0.0, *0.0*
	1CH_2pyrrolidine$^+$	41.6, *41.2*	42.9, *42.1*	36.0, *36.2*
	H^+1$CH_3$3Pyr[N]	62.0, *62.2*	62.8, *62.4*	55.4, *51.2*
	H^+1$CH_3$2Pyr[N]	63.9, *64.1*	64.4, *63.9*	57.9, *54.2*
$Li^+(C_5H_9N)$	Li^+2$CH_3$1Pyr[N]	0.0, *0.0*	0.0, *0.0*	0.0, *0.0*
	Li^+3$CH_3$1Pyr[N]	33.7, *34.8*	33.3, *35.4*	29.1, *27.7*
	Li^+1$CH_3$2Pyr[N]	108.2, *107.1*	107.9, *106.4*	103.0, *100.3*
	Li^+1$CH_3$3Pyr[N]	113.1, *112.7*	112.3, *111.5*	105.7, *103.9*
	Li^+1$CH_3$2Pyr[C3]	126.5, *124.2*	125.2, *122.5*	131.6, *129.2*

[a]Structure optimizations and zero-point corrections calculated at the B3LYP/6-311G+(d,p) level of theory. Single point energies listed at the three levels of theory are calculated using the 6-311+G(2d,2p) basis set. Values in italics indicate geometry optimizations done at the MP2(full)/cc-pVDZ(Li-C) level with single point energies calculated at the indicated levels using the aug-cc-pVTZ(Li-C) basis set.

Table 2. Relative energies (kJ/mol) of intermediates, transition states, and products for Li^+(Pro) decomposition relative to the ground conformer.[a]

Structure	theory (kJ/mol)		
	B3LYP	B3P86	MP2(full)
Loss of CO			
[CO_2^-] C4-up,c	0.0, *0.0*	0.0, *0.0*	0.0, *0.0*
TS[CO_2^--CO] C4-up,c	36.4, *32.7*	29.8, *26.4*	39.0, *33.5*
[CO] C4-up,c	40.2, *35.6*	36.9, *31.0*	44.9, *39.2*
TS [CO] C(4-5)-up,(ct)	105.7, *103.3*	106.9, 104.3	113.6, *112.1*
[CO] C5-up,t	92.6, *90.4*	93.5, *91.2*	101.3, *101.0*
TS[CO] C(5-3)-(up-down),t	96.3, *93.6*	97.4, *94.6*	104.9, *104.1*
[CO] C3-down,t	95.3, *93.4*	96.3, *94.3*	103.2, *102.6*
TS[CO-COOH] C3-down,t	99.1, *98.2*	99.5, *98.7*	104.0, *105.8*
[COOH] C3-down,t	99.6, *99.2*	100.5, *100.5*	103.7, *105.8*
TS[OH]{C2~CO~OH}	**205.5, *204.9***	**242.4, *238.3***	**240.9, *264.0***
(2Pyr[C3])H^+($LiOH_H$) + CO	176.5, *173.2*	221.9, *219.2*	202.7, *234.2*
TS(H^+2Pyr[C3])($LiOH_{H-C2}$) + CO	179.9, *174.8*	227.5, *221.1*	202.4, *234.2*
H^+2Pyr[C3] C4-down($LiOH_{C2}$) + CO	160.1, *158.6*	189.3, *187.9*	163.9, *187.6*
TS(H^+2Pyr[C3]C4(down-up))($LiOH_{C2}$) + CO	163.0, *165.5*	193.5, *194.9*	170.5, *193.1*
H^+2Pyr[C3]C4-up($LiOH_{C2}$) + CO	151.6, *150.6*	180.6, *179.5*	153.1, *177.6*
TS(H^+2Pyr[C3])($LiOH_{C2-NH}$) + CO	170.2, *168.6*	218.7, *217.9*	194.6, *229.1*
H^+2Pyr[C3]($LiOH_{NH}$) + CO	96.7, *96.6*	137.1, *139.1*	106.4, *141.0*
Loss of LiOH			
H^+2Pyr[C3] + CO + LiOH	**252.2, *249.6***	**306.4, *305.2***	**282.2, *319.4***

Loss of H_2O			
TS(2-1)($Pyr_{H\text{-}Li}$)$Li^+(H_2O)$ + CO	111.9, *110.2*	154.0, *153.9*	119.4, *153.8*
(1Pyr[N])$Li^+(H_2O)$ + CO	41.4, *39.4*	90.3, *90.1*	51.0, *90.2*
Li^+1Pyr[N] + CO + H_2O	150.4, *149.0*	195.1, *195.5*	162.4, *200.0*
Loss of Proline			
Li^+ + Pro	**266.6, *268.0***	**258.1, *259.7***	**260.3, *262.5***
Li^+ + 1Pyr[N] + CO + H_2O	349.6, *349.6*	389.0, *391.0*	355.3, *393.0*

[a]Geometry optimizations and vibrational frequencies calculated at the B3LYP/6-311+G(d,p) level of theory. Single point energies are calculated at indicated levels using the 6-311+G(2d,2p) basis set and include zero-point corrections. Values in italics indicate optimizations done at the MP2(full)/cc-pVDZ(Li-C) level with single point energies at the shown levels using the aug-cc-pVTZ(Li-C) basis set. Values in bold indicate the rate limiting TS for that channel.

UU IR Author Manuscript

Table 3. Relative energies (kJ/mol) of intermediates, transition states, and products for Li^+(NMP) decomposition relative to the ground conformer.[a]

structure	theory (kJ/mol)		
	B3LYP	B3P86	MP2(full)
Loss of LiOH			
TS[OH]{C2~CO~OH}	191.7, *192.2*	229.4, *225.9*	**230.4**, *254.3*
$(1CH_32Pyr[C3])H^+(LiOH_H)$ + CO	165.9, *168.9*	212.6, *217.9*	192.2, *222.9*
$TS(H^+1CH_32Pyr[C3])(LiOH_{H\text{-}C2})$ + CO	167.8, *163.8*	216.1, *211.5*	191.3, *228.4*
$H^+1CH_32Pyr[C3](LiOH_{C2})$ + CO	157.0, *172.7*	203.2, *202.8*	178.1, *209.3*
$TS(H^+1CH_32Pyr[C3])(LiOH_{C2\text{-}C2H})$ + CO	158.4, *160.1*	207.1, *209.3*	181.9, *220.4*
$H^+1CH_32Pyr[C3](LiOH_{C2H})$ + CO	148.0, *148.4*	194.5, *195.8*	170.1, *208.6*
$H^+1CH_32Pyr[C3]$ + CO + LiOH	**232.7, *230.2***	**286.9, *286.0***	**266.5, *305.8***
Loss of H_2O			
$TS(1CH_32Pyr)H^+_{C3\text{-}OH}(LiOH)$ + CO	174.6, *168.7*	211.3, *208.1*	198.8, *232.7*
$(1CH_32Pyr_H)(H_2O)Li^+$ + CO	178.4, *176.6*	216.1, *215.7*	195.2, *228.8*
$TS(1CH_32Pyr_{H\text{-}Li})Li^+(H_2O)$ + CO	187.3, *183.7*	225.3, *222.7*	205.2, *239.1*
$(1CH_32Pyr[N])Li^+(H_2O)$ + CO	110.8, *107.6*	156.8, *154.7*	117.3, *156.3*
$Li^+1CH_32Pyr[N]$ + CO + H_2O	**217.1, *214.6***	**258.8, *257.8***	229.8, ***266.5***
$Li^+(H_2O)$ + CO + $1CH_32Pyr$	**248.2, *243.8***	**290.2, *324.9***	**263.1, *301.3***
Loss of NMP			
Li^+ + NMP	**281.1, *281.7***	**272.1, *272.5***	**268.7, *277.8***
$Li^+ + 1CH_32Pyr + CO + H_2O$	387.3, *384.5*	424.4, *423.5*	397.9, *436.3*

[a]Geometries and vibrational frequencies calculated at B3LYP/6-311+G(d,p) level of theory. Single point energies are calculated at indicated levels using the 6-311+G(2d,2p) basis set and include zero-point corrections. Values in italics indicate optimizations done at MP2(full)/cc-pVDZ(Li-C) level with single point energies at the shown levels using the aug-cc-pVTZ(Li-C) basis set. Values in bold indicate the rate limiting TS for that channel.

Table 4. Fitting parameters of Eq. (1), threshold dissociation energies at 0 K, and entropies of activation at 1000 K for CID of Li^+(Pro) and Li^+(NMP) with Xe.[a]

reactant	product		*n*	E_0 (eV)	$\Delta S^{\dagger}_{1000}$ (J/mol K)
Li^+(Pro)	Li^+ + Pro	2.4 (0.2)	1.5 (0.2)	2.80 (0.09)[b]	37 (2)
Li^+(Pro)	sum (CO + H_2O/LiOH)	2.8 (0.9)	1.6 (0.2)	2.51 (0.14)	82 (1)
Li^+(Pro)[c,d]	sum (CO + H_2O/LiOH)	2.6 (0.8)	1.6 (0.3)	2.06 (0.09)	-39 (3)
	Li^+ + Pro	3.6 (5.0)	1.6 (0.3)	2.67 (0.05)	43 (2)
Li^+(Pro)[e]	Li^+1Pyr[N] + CO + H_2O	1.3 (0.2)	1.6 (0.2)	2.34 (0.08)	82 (1)
	H^+2Pyr[C3] + CO + LiOH	1.1 (0.1)	1.6 (0.2)	<2.90 (0.09)	-9 (4)
Li^+(Pro)[d,e]	Li^+1Pyr[N] + CO + H_2O	1.3 (0.3)	1.6 (0.3)	1.96 (0.07)	-39 (3)
	H^+2Pyr[C3] + CO + LiOH	1.1 (0.2)	1.6 (0.3)	<2.84 (0.05)	-9 (4)
Li^+(Pro)[c,d,e]	Li^+1Pyr[N] + CO + H_2O	2.5 (0.7)	1.6 (0.2)	2.05 (0.07)	-39 (3)
	H^+2Pyr[C3] + CO + LiOH	2.2 (0.5)	1.6 (0.2)	<2.86 (0.12)	-7 (5)
	Li^+ + Pro	2.5 (0.7)	1.6 (0.2)	2.64 (0.07)	43 (2)
Li^+(NMP)	Li^+ + NMP	0.1 (0.03)	2.2 (0.2)	3.39 (0.17)	49 (3)
Li^+(NMP)	Li^+ + NMP	0.6 (0.08)	0.8 (0.1)	4.10 (0.16)	48 (3)
Li^+(NMP)	sum (CO + H_2O/LiOH)[f]	7.3 (1.6)	1.6 (0.2)	2.56 (0.06)	91 (1)
Li^+(NMP)[c,d]	sum (CO + H_2O/LiOH)[g]	15.5 (3.9)	0.8 (0.2)	2.63 (0.11)	42 (1)
	Li^+ + NMP	14.3 (5.7)	0.8 (0.2)	3.45 (0.11)	49 (3)
Li^+(NMP)[e]	Li^+1$CH_3$2Pyr[N] + CO + H_2O	7.8 (1.4)	1.6 (0.2)	2.58 (0.07)	91 (1)
	H^+1$CH_3$2Pyr[C3] + CO + LiOH	7.3 (1.2)	1.6 (0.2)	<3.07 (0.11)	-3 (4)
Li^+(NMP)[d,e]	Li^+1$CH_3$2Pyr[N] + CO + H_2O	6.3 (1.1)	1.9 (0.3)	2.34 (0.05)	42 (1)
	H^+1$CH_3$2Pyr[C3] + CO + LiOH	6.0 (1.0)	1.9 (0.3)	<3.07 (0.10)	-3 (4)

[a]Uncertainties (one standard deviation) are listed in parentheses. [b]When the lifetime effect is not included, the threshold of Li^+ increases to 3.61 (0.08) eV. [c]Competitive analysis using a tight TS for CO loss for the cross section sum and a PSL TS for Li^+ cross section. [d]Scaling factors for the frequencies below 1000 cm^{-1} of the tight TS for CO loss are 2 ± 0.2 for Li^+(Pro) and 1.26 ± 0.02 for Li^+(NMP). [e]Competitive analysis using a tight TS for CO loss and a PSL TS for LiOH loss treated as a sequential dissociation after CO loss. [f]Cross section sum analyzed up to 5 eV using the tight TS for CO loss. [g]Cross section sum analyzed over energy range of 1 – 9 eV.

Table 5. Comparison of experimental and theoretical energies (kJ/mol) of transition states and fragmentation complexes of lithiated proline and NMP at 0 K.

ionic product	experiment	Theory		
	TCID[a]	B3LYP[b]	B3P86[b]	MP2(full)[b]
TS[OH]{C2~CO~OH}	198 ± 7	206, *205*	242, *238*	241, *264*
Li^+1Pyr[N] + CO + H_2O		150, *149*	195, *196*	162, *200*
H^+2Pyr[C3] + CO + LiOH	<276 ± 12	252, *250*	306, *305*	282, *319*
Li^+ + Pro	255 ± 7	267, *268*	258, *260*	260, *262*
TS[OH]{C2~CO~OH}	226 ± 5	192, *192*	229, *226*	230, *254*
Li^+1$CH_3$2Pyr[N] + CO + H_2O		217, *215*	259, *258*	230, *266*
H^+1$CH_3$2Pyr[C3] + CO + LiOH	<296 ± 10	233, *230*	287, *286*	266, *306*
Li^+ + NMP	264 ± 13[c]	281, *282*	272, *272*	269, *278*
MAD[d]		18, *18*	15, *13*	14, *29*
MAD[e]		26, 27	17, *16*	16, *28*

[a]Present results taken from Table 4. [b]Energies calculated at the corresponding 6-311+G(2d,2p)//B3LYP/6-311+G(d,p) level. Zero point energies are included for all values, and counterpoise corrections for BSSE are included for Li^+-AA bond energies. Values in italics indicate energies calculated at the corresponding aug-cc-pVTZ(Li-C)//MP2(full)/aug-cc-pVDZ(Li-C) level without BSSE corrections. [c]Li^+ threshold energy estimated by as described in text. [d]Mean absolute deviation (MAD) from four experimental threshold energies excluding those for LiOH. [e]Mean absolute deviation (MAD) from all six experimental threshold energies.

Figure Captions

Fig. 1. Cross sections for CID of Li^+(Pro) (part a) and Li^+(NMP) (part b) with Xe (zero pressure extrapolated and 0.20 mTorr, respectively) as a function of kinetic energy in the center-of-mass frame (lower x-axis) and the laboratory frame (upper x-axis).

Fig. 2. Structures of the ground conformers of the Li^+(AA) reactants where AA = Pro and NMP and optimized structures of products formed by loss of (CO + LiOH) and (CO + H_2O), calculated at the MP2(full)/cc-pVDZ(Li-C) level. Relative energies in kJ/mol calculated at MP2(full)/6-311+G(2d,2p) level with ZPE corrections included are shown for X = H (X = CH_3). The product ions and energies calculated for Li^+(NMP) are indicated within parentheses.

Fig. 3. Potential energy surface for the lowest-energy pathway for the loss of H_2O and LiOH from Li^+(Pro) starting from TS[OH]{C2~CO~OH} calculated at the MP2(full)/6-311+G(2d,2p)//B3LYP/6-311+G(d,p) level. All species except this TS are also accompanied by the initial CO product. The notation describing each TS and intermediate is described in the text.

Fig. 4. Potential energy surface for the lowest-energy pathway for the loss of H_2O and LiOH from Li^+(NMP) starting from TS[OH]{C2~CO~OH} calculated at the MP2(full)/6-311+G(2d,2p)//B3LYP/6-311+G(d,p) level. All species except this TS are also accompanied by the initial CO product. The notation describing each TS and intermediate is described in the text.

Fig. 5. Competitive analysis of the cross sections for Li^+ and cross section sum for Li^+(Pro) (part a) and Li^+(NMP) (part c). Part b shows a combined competitive and sequential fit for all three decompositions for Li^+(Pro). Part d shows a competitive analysis of the cross sections for $Li^+1CH_32Pyr[N]$ + CO + H_2O and $H^+1CH_32Pyr[C3]$ + CO + LiOH (TL model). Experimental data is shown by open symbols. Solid lines show the best fit to the experimental data using the model of Eq. (1) and the sequential model, convoluted over the neutral and ion kinetic and internal energy distributions. Dashed lines show the model cross sections in the absence of experimental kinetic energy broadening for reactants with an internal energy of 0 K.

UU IR Author Manuscript

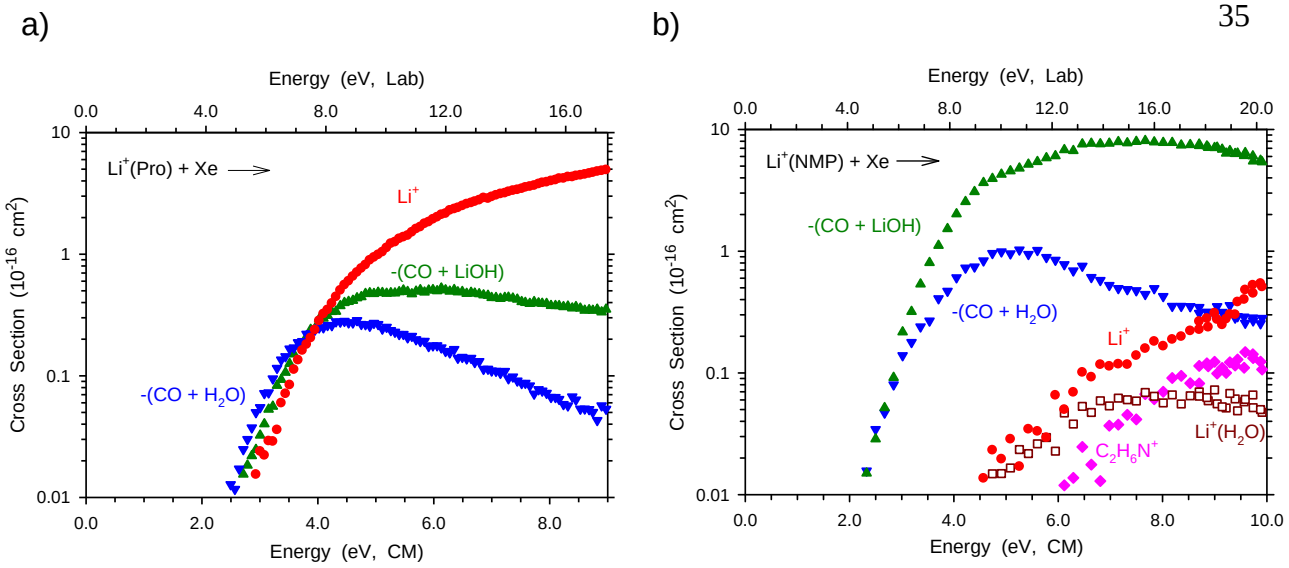

Figure 1

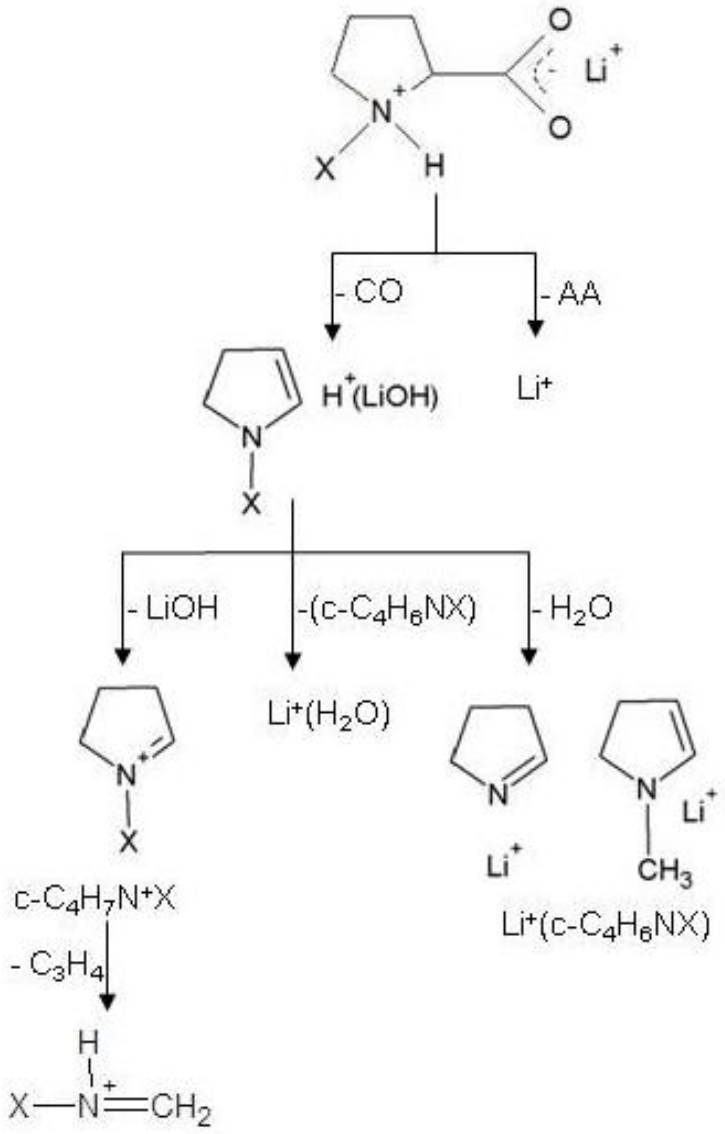

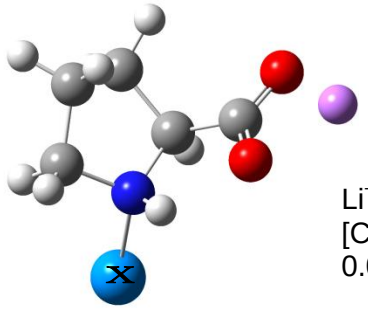

Li^+(AA)
[CO_2^-] C4-up,c
0.0 (0.0)

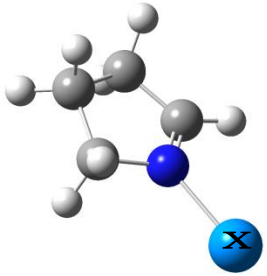

H^+2Pyr [C3]
($H^+1CH_3$2Pyr[C3])
0.0 (0.0)

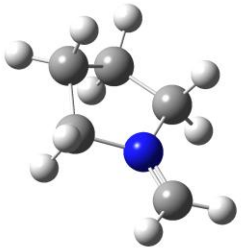

(1CH_2pyrrolidine)$^+$
(36.0)

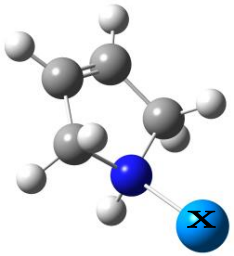

H^+3Pyr [N]
($H^+1CH_3$3Pyr[N])
41.1 (55.4)

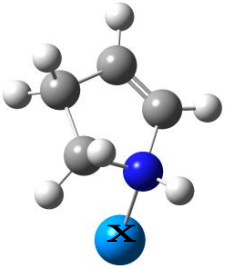

H^+2Pyr [N]
($H^+1CH_3$2Pyr[N])
46.5 (57.9)

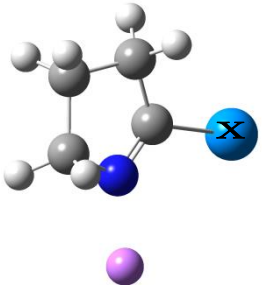

Li^+1Pyr [N]
($Li^+2CH_3$1Pyr[N])
0.0(0.0)

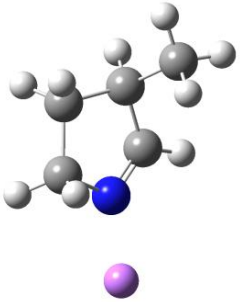

($Li^+3CH_3$1Pyr[N])
(29.1)

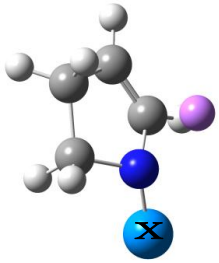

Li^+2Pyr [N]
($Li^+1CH_3$2Pyr[N])
56.3 (103.0)

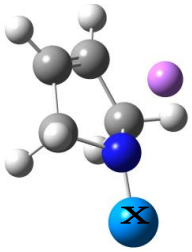

Li^+3Pyr [N]
($Li^+1CH_3$3Pyr[N])
57.6 (105.7)

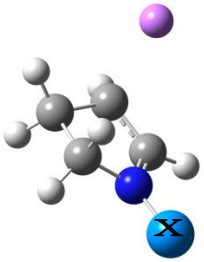

Li^+2Pyr [C3]
($Li^+1CH_3$2Pyr[C3])
88.9 (131.6)

Figure 2

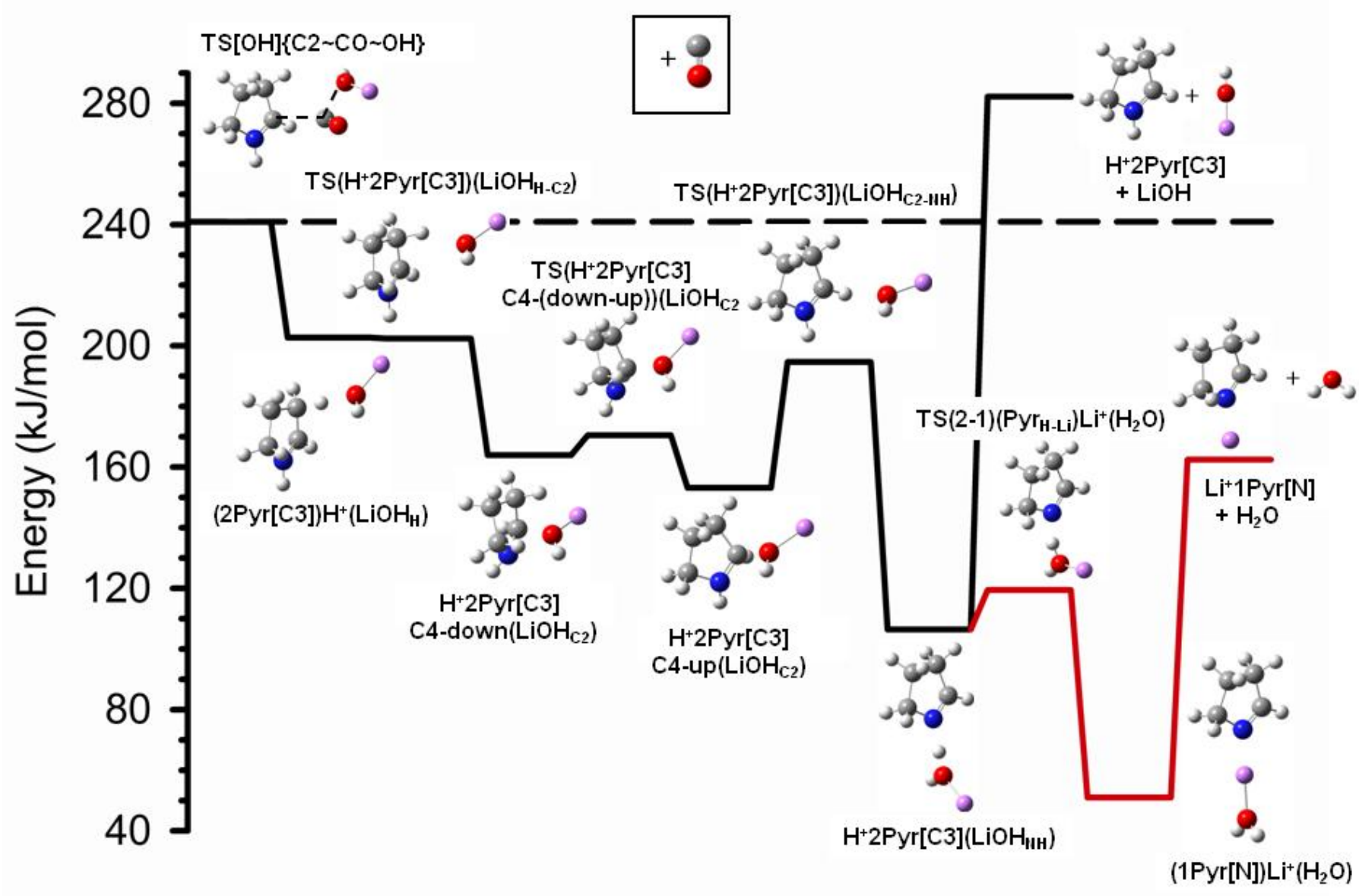
Energy (kJ/mol)
280
240
200
160
120
80
40
TS[OH]{C2~CO~OH}
TS(H+2Pyr[C3])(LiOHH-C2)
TS(H+2Pyr[C3])(LiOHC2-NH)
H+2Pyr[C3]
+ LiOH
TS(H+2Pyr[C3]
C4-(down-up))(LiOHC2
(2Pyr[C3])H+(LiOHH)
H+2Pyr[C3]
C4-down(LiOHC2)
H+2Pyr[C3]
C4-up(LiOHC2)
TS(2-1)(PyrH-Li)Li+(H2O)
Li+1Pyr[N]
+ H2O
H+2Pyr[C3](LiOHNH)
(1Pyr[N])Li+(H2O)

Figure 3

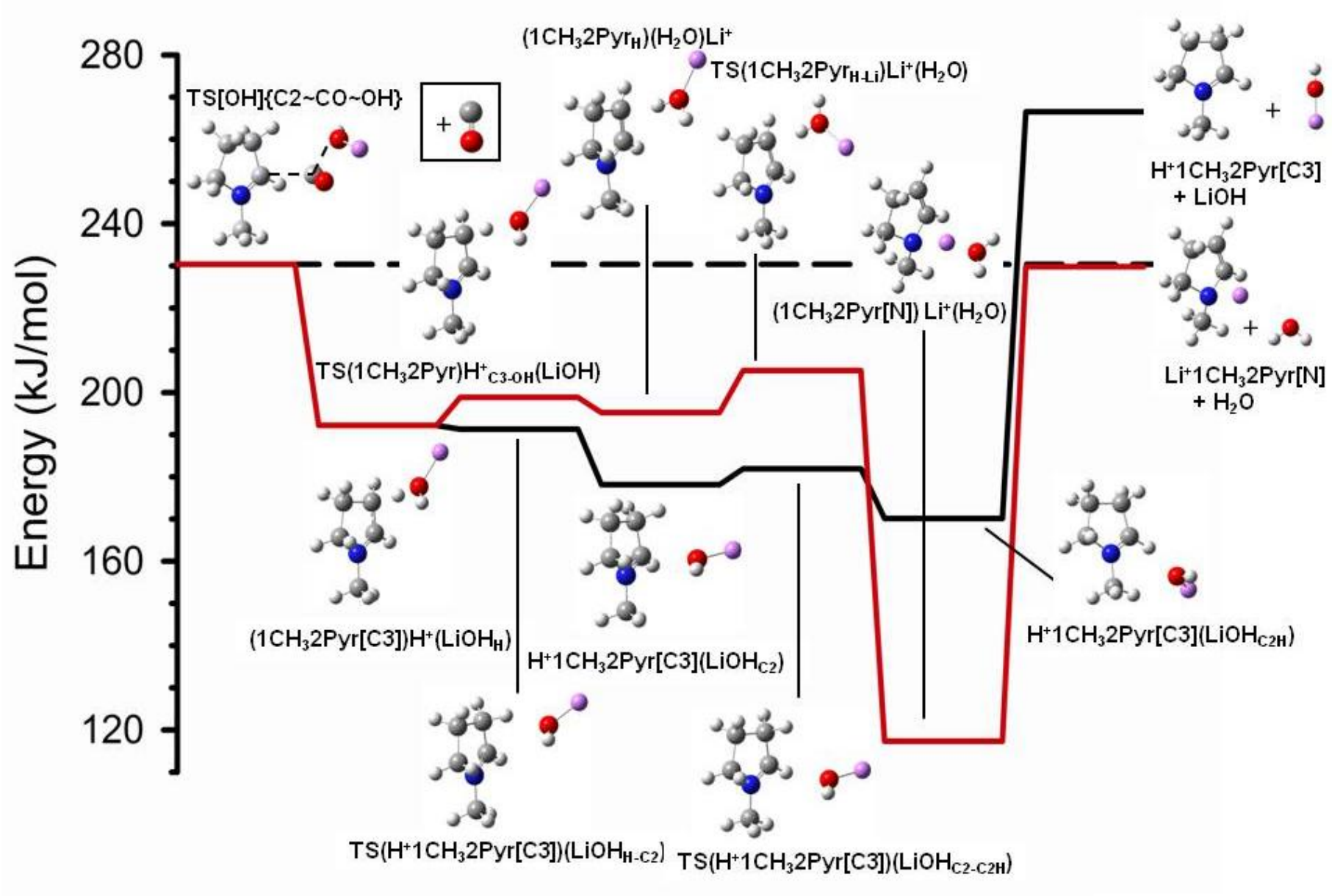
Energy (kJ/mol)
280
240
200
160
120
TS[OH]{C2~CO~OH}
(1CH3 2Pyr H)(H2O)Li+
TS(1CH3 2Pyr H-Li)Li+(H2O)
H+1CH3 2Pyr[C3] + LiOH
(1CH3 2Pyr[N]) Li+(H2O)
Li+1CH3 2Pyr[N] + H2O
TS(1CH3 2Pyr)H+C3-OH(LiOH)
(1CH3 2Pyr[C3])H+(LiOHH)
H+1CH3 2Pyr[C3](LiOHC2)
H+1CH3 2Pyr[C3](LiOHC2H)
TS(H+1CH3 2Pyr[C3])(LiOHH-C2)
TS(H+1CH3 2Pyr[C3])(LiOHC2-C2H)

Figure 4

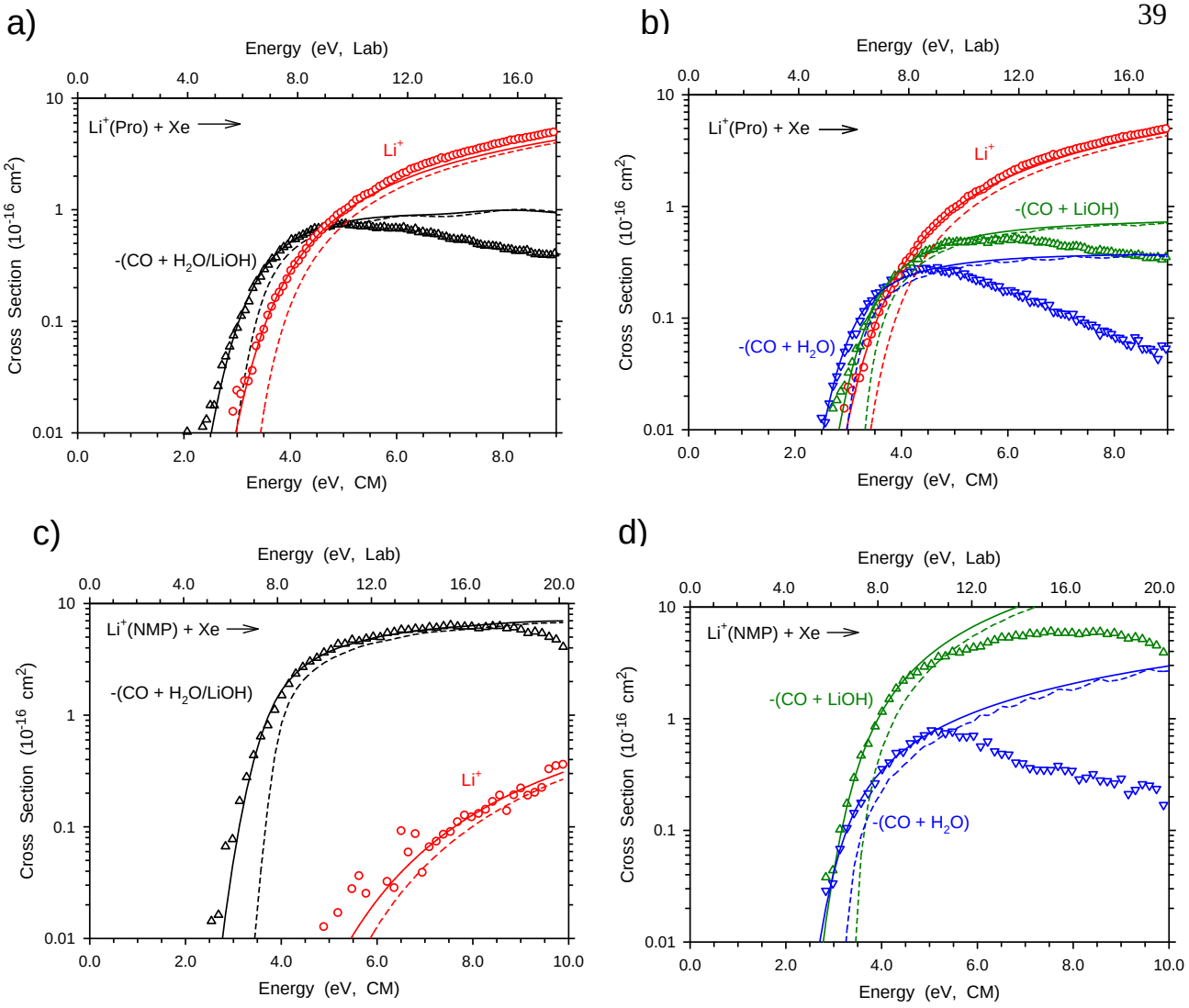

Figure 5